



Special Feature: Nano Structured Devices

Research Report

Fabrication of Periodic Structures by Self-assembly: An Adaptable Strategy for Wide Implementation in Nanodevices

Yuri Yamada, Kota Ito, Tadashi Nakamura, Atsushi Miura and Kazuhisa Yano

Report received on Jul. 22, 2019

■ABSTRACT■ Self-assembly is a promising and simple strategy to produce nanostructures. Components autonomously assemble into an organized pattern without the need for specific fabrication devices. Here we present the fabrication and application of two types of SiO₂ nanostructures by taking advantage of self-assembly. One consists of colloidal photonic crystals fabricated from monodisperse mesoporous silica spheres (MMSS), which have ordered hexagonal mesopores and high monodispersity. Reversible control of light reflection and changes of the corresponding structural colors are demonstrated simply by changing the amount of water vapor adsorbed within the mesopores. The introduction of an organic dye, Rhodamine, into the mesopores of MMSS colloidal crystals enabled the manipulation of spontaneous emission from Rhodamine, which can be used to realize efficient light-matter interaction. The other nanostructure is an array of SiO₂ nanopillars that have sub-30 nm diameter and a height of 200 nm, which was obtained by self-assembly of a polystyrene-*block*-poly(dimethylsiloxane) (PS-*b*-PDMS). A substrate-scale (ca. 4 cm²) uniformity of the nanofeature structures was adopted as a reproducible surface-enhanced Raman spectroscopy (SERS) substrate with enhanced signal intensity via sputtering of a thin Au layer on the top of SiO₂ nanopillars. Fabrication of nanostructures using self-assembly is cost-effective and time-efficient, and can thus offer a simple solution to realize an affordable nanofabrication technology that will contribute to significant advances in nanotechnology.

■KEYWORDS■ Self-assembly, Nanostructure, Photonic Crystal, SERS, Hexagonal Regularity, Thin Film

1. Introduction

Nanotechnology has recently achieved much research significance, and advances in nanostructured materials are paving the way for a variety of applications in electronics, information technology, and medicine.⁽¹⁻⁴⁾ Manufacturing technology is crucial for developments in these fields and is classified into two main categories: top-down and bottom-up approaches. Both approaches have advantages and disadvantages, and significant efforts are underway to develop applicable fabrication methods using both approaches. The top-down approach includes various lithographical methods to pattern nanoscale structures. Representative methods are photolithography and scanning beam (or maskless) lithography, which have contributed significantly to the integration of semiconductors and electronic devices.^(5,6) However, these processes are becoming increasingly more difficult and expensive as the size scale of device features approaches the diffraction

limit of light.

In contrast, the bottom-up approach utilizes physicochemical interactions to regulate various building blocks such as atoms, molecules, and their assembled small units, which leads to novel supramolecular architectures.^(7,8) Self-assembly, in which building blocks spontaneously form into an organized pattern or structure without the need for specific fabrication devices, has significant potential for the fabrication of next-generation nanodevices. Self-assembly is simple, low cost, and time effective, and can thus overcome the drawbacks of the top-down strategy. One well-known example of self-assembly is gem opals, which are composed of ordered spherical silica nanoparticles formed through the sedimentation and compression of siliceous substances under natural hydrostatic and gravitational forces over a long period. Inspired by gem opals and other naturally created structures, the design and fabrication of nanofeatured materials by self-assembly has been intensively proposed.^(9,10) In

particular, the self-assembly of monodisperse colloids of dielectric materials into closed packed structures has been investigated for the preparation of colloidal photonic crystals.⁽¹¹⁾ Photonic crystals are dielectric materials with spatial periodicity comparable to that of electromagnetic waves.⁽¹²⁾ Sufficient dielectric contrast and appropriate geometry yield a photonic band gap (PBG) where the propagation of light is strictly inhibited. There have been many pioneering works that have demonstrated unique properties, such as the strong localization of photons, the suppression or enhancement of light emission, and the manipulation of spontaneous emission.⁽¹³⁻¹⁵⁾

Another promising research area that employs self-assembly is mesoporous materials, where sol-gel chemistry and the micelle formation of surfactant molecules are successfully combined.⁽¹⁶⁾ The self-assembled surfactants serve as pore-directing agents, and inorganic precursors are subsequently or simultaneously condensed around them. The most commonly studied mesoporous material is mesoporous silica with periodically ordered pores in the range of 2-50 nm. Mesoporous silica is a prominent candidate for emerging applications such as catalysis and energy harvesting due to its large surface areas and tunable pore sizes.^(17,18)

We have further utilized the concept of self-assembly and demonstrated the synthesis of monodisperse mesoporous silica spheres (MMSS) and the fabrication of photonic colloidal crystals from MMSS.⁽¹⁹⁻²¹⁾ Three-dimensional opal-like close-packed crystals were strategically obtained by the self-assembly of MMSS due to the high monodispersity of the particles that were endowed with ordered mesopores, which were templated by self-assembled surfactants. Here, we present novel properties and unique applications using photonic colloidal crystals fabricated from MMSS, which are regarded as MMSS synthetic opals analogous to natural gem opals.

A variety of surfactants, such as ionic and neutral surfactants, and their mixtures, can be used for the synthesis of mesoporous materials. One typical example of a neutral surfactant is a block polymer, where immiscible polymer chains are covalently or non-covalently linked to each other. They can spontaneously form microphase-separated structures with domain sizes of approximately several tens of nanometers and a variety of morphologies.⁽²²⁾ Controllable variation in size and morphology has

resulted in the self-assembly of block copolymers in many applications, apart from mesoporous silica chemistry.⁽²³⁾

We have recently demonstrated the fabrication of a SiO₂ perpendicular nanopillar array, with a pillar diameter of 30 nm, from the self-assembly of a Si-containing block copolymer, polystyrene-*block*-poly(dimethylsiloxane) (PS-*b*-PDMS).⁽²⁴⁻²⁶⁾ Highly aligned hexagonal patterns consisting of perpendicular nanopillars were obtained over a substrate (ca. 4 cm²) via a simple process. The SiO₂ nanopillar arrays exhibit unique properties that can be applied to nanophotonic devices, which are also introduced in this study.

2. Experimental

2.1. MMSS Synthetic Opals

2.1.1. Preparation of MMSS and Fabrication of Synthetic Opals

We have modified the Stöber method, which employs a water-alcohol-ammonia-alkoxysilane system, to obtain monodisperse spherical particles that result from minimization of the surface energy.⁽²⁷⁾ Hexadecyltrimethylammonium bromide (C₁₆TMABr) was added to this system as a pore directing agent. At first, C₁₆TMABr was dissolved in a methanol/water mixture under basic conditions to obtain a clear solution. The solution turned opaque suddenly after the addition of tetramethyl orthosilicate (TMOS) as a silica source, under vigorous stirring at 298 K. A white powder was obtained after filtration and repeated washing, followed by the removal of organic substances at 823 K for 6 h to yield MMSS (**Fig. 1(a)**).⁽²⁸⁾

A fluidic cell was adopted to promote the self-assembly of MMSS to form synthetic opals. The cell was composed of two flat glass slides placed 30 μm apart using double-sided tape.⁽²⁹⁾ The capillary force was utilized to introduce an aqueous dispersion of MMSS (10 wt%), and synthetic opals were obtained after the gradual evaporation of water from the opening of the cell at room temperature. The top glass slide was carefully removed to unveil the opal films for further measurements.

2. 1. 2. Fabrication of MMSS Synthetic Opals Impregnated with Fluorescent Guests

MMSS with diameters of 320 or 564 nm were used, and [9-(2-Carboxyphenyl)-6-(diethylamino)xanthen-3-ylidene]-diethylazanium hydrochloride (Rhodamine B: Rh B) was selected as a fluorescent guest (fluorophore). Rh B was dissolved in ethanol (1.25-5 mM) and 0.2 g of MMSS was added. The suspension was shaken overnight at ambient temperature to reach adsorption equilibrium. The Rh B-MMSS conjugate was collected by centrifugation and dried at room temperature. In this study, 100 mg of MMSS was prepared, the mesopores of which were filled with 0.2 mg of Rh B. A 1 wt% of the Rh B-MMSS conjugates was dispersed in water and introduced into the fluidic cell in the same manner as in Sec. 2.1.1, to yield an Rh B-MMSS opal.⁽²¹⁾

2. 1. 3. Characterization

The morphology of the MMSS was investigated using scanning electron microscopy (SEM: S-3600N, Hitachi High-Technologies Corp.) at an acceleration voltage of 10 kV. The surfaces of the samples were coated with gold to facilitate SEM observations.

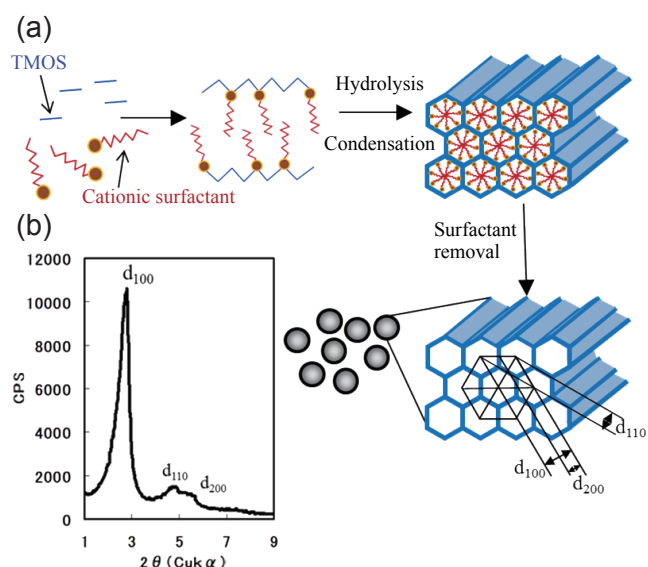


Fig. 1 (a) A schematic illustration of synthetic route for monodispersed mesoporous silica spheres (MMSS). (b) An XRD pattern of MMSS, indicating a presence of an ordered hexagonal mesoporous structure.

The regularity of the mesopores of the MMSS was confirmed by X-ray diffraction (XRD: Rint-2200, Rigaku) measurements using Cu $K\alpha$ radiation. Water adsorption/desorption isotherms (Belsorp-18, MicrotracBEL) were measured at 298 K in a static water vapor system. Photoluminescence spectra were measured using a spectrometer (FP-6500, Jasco).

2. 1. 4. Control of Light Reflection Using Water Vapor Adsorption

To demonstrate that light reflection can be controlled by the adsorption properties of MMSS opals, angle-resolved reflection spectra were measured using multichannel spectrometers (Fastevert S-2650 and S-2710, Soma Optics). Prior to the measurements, the film was evacuated for five hours at 323 K to remove water present in the interplanar spacings and in the mesopores. **Figure 2** shows a schematic diagram of the experimental setup for the measurement.⁽¹⁹⁾ The MMSS opal was set in a glass container, into which water vapor was introduced using nitrogen as a carrier gas. The relative water vapor pressure was monitored and reflection spectra were collected at $P/P_0 = 0.2, 0.4,$ and 0.8 while changing the incidence angle θ between the beam and the direction normal to the film surface.

2. 1. 5. Manipulation of Spontaneous Emission

Amplified spontaneous emission was investigated using the experimental setup depicted in **Fig. 3**. Rh B-MMSS opals were set on a stage surrounded by a circular θ stage that was connected to an optical fiber through a movable arm. The sample position and direction of the excitation laser were fixed, and angle-resolved emission spectra were investigated by

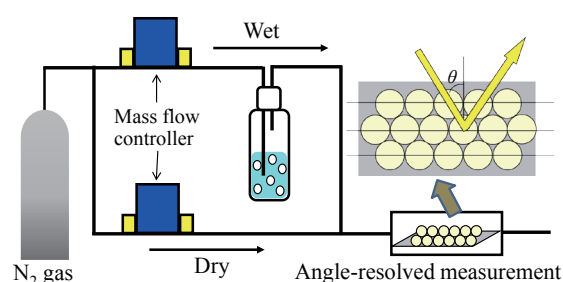


Fig. 2 A schematic diagram of the experimental setup for an angle-resolved reflection spectra measurement.

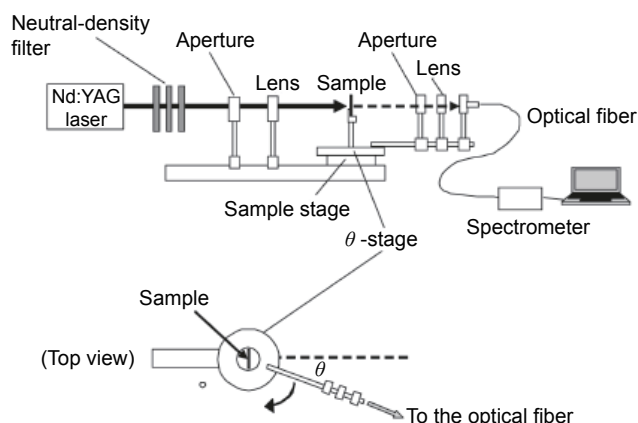


Fig. 3 A schematic illustration of an optical setup used in the emission studies. Angle-resolved emission spectra can be collected by changing the detector angle θ .

changing θ . The sample was excited using the second harmonic of a pulsed Nd:YAG laser (532 nm) with the pulse energy controlled by neutral-density filters and the aperture. The pulse duration and repetition frequency of the laser were 3 ns and 10 Hz, respectively. The spot size of the laser beam was 1 mm, which was focused down to 100 μm on the sample surface using a lens with a focal length of 150 mm. The emission from the sample was collected and focused onto the entrance of the optical fiber connected to a spectrometer (HR4000, Ocean Optics).

2. 2. Silica Nanopillars

2. 2. 1. Self-assembly of PS-*b*-PDMS

Figure 4 shows a schematic representation of the overall process for the preparation of microphase-separated nanopillars.⁽²⁵⁾ A solution of 3-5 wt% PS-*b*-PDMS with a molecular weight of 45.5 kg mol⁻¹ (31k-*b*-14.5k) dissolved in tetrahydrofuran (THF) was spin-cast on a Si substrate. According to the volume ratio, the minor component of PDMS forms microdomains within the matrix of the major component, PS. The film was annealed in saturated chloroform vapor in a closed glass chamber, which induced microphase separation. The film was then rapidly removed from the chamber to quench the structure. PDMS wetting layers form on the top surface due to the low surface

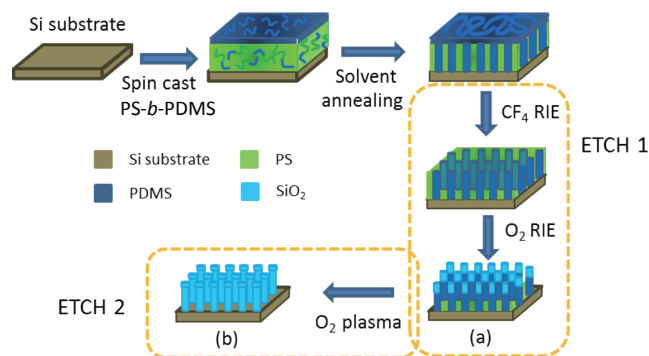


Fig. 4 A schematic representation of fabrication process of SiO₂ nanopillar arrays.

energy of PDMS with respect to that of PS. Two-step reactive ion etching (RIE) was conducted using tetrafluoromethane (CF₄) to remove the PDMS surface layer, followed by O₂ RIE to partially etch the organic components and oxidize PDMS to SiO_x (ETCH 1 in Fig. 4). O₂ plasma treatment using a plasma reactor (PR300, Yamato Science Co. Ltd.) was then conducted to completely remove organic substances and leave the silica (SiO₂) pillar arrays on the substrate (ETCH 2 in Fig. 4). Transient and final morphologies were investigated by surface and cross-sectional SEM observation using field-emission scanning electron microscopy (S-4800 and S-5500, Hitachi). Unless otherwise noted, SEM images were acquired after the ETCH 1 process (sample (a) in Fig. 4).

2. 2. 2. Application as Surface-enhanced Raman Spectroscopy (SERS) Platform

A gold (Au) layer with a thickness of 8 nm was deposited on the surface of the SiO₂ nanopillar arrays by electron-beam evaporation (EVD-500B, Anelva) with a background pressure of 9.7×10^{-5} Pa to form a surface-enhanced Raman spectroscopy (SERS) platform. A thin titanium layer was deposited beforehand to improve the adhesion between SiO₂ and Au. A flat Au film was fabricated on the Si substrate in the same manner and used as a control sample. A 5×10^{-6} M solution of ethyl 2-[3-(ethylamino)-6-ethylimino-2,7-dimethylxanthen-9-yl]benzoate hydrochloride (Rhodamine 6G; R6G) was prepared, in which the substrates were immersed for 0.5 h, followed

by rinsing with deionized water to remove R6G molecules that were not adsorbed. SERS measurements were performed using a laser Raman spectrometer (NRS-3300, Jasco Ltd.) with an excitation wavelength of 532 nm. The intensity of the laser beam was less than 0.1 mW and 90 laser shots were summed to produce one spectrum with an exposure time of 1 s.⁽²⁵⁾

3. Results and Discussion

3. 1. MMSS Synthetic Opals

3. 1. 1. Primitive Properties of MMSS

The XRD pattern for MMSS has a sharp peak assigned to (100) planes, in addition to higher order diffraction peaks, which indicates the MMSS has highly ordered hexagonal pores that can host various molecules (Fig.1(b)). **Figure 5** shows SEM images of MMSS and the fabricated opal film. Spherical morphology with an average particle size of 473 nm and a standard deviation of 4.0% was confirmed for MMSS (Fig. 5(a)), which indicates high monodispersity. The size uniformity enables MMSS to self-organize into three-dimensional periodic crystals with a macroscopic size. The MMSS opal film has a high degree of ordered face-centered cubic (fcc) structure with the (111) plane oriented parallel to the

substrate, as shown in Fig. 5(b). When light is incident on a colloidal crystal, propagation of the reflected light (λ_{peak}) is governed by Bragg's law:⁽³⁰⁾

$$\lambda_{\text{peak}} = 1.633d(n_{\text{eff}}^2 - \sin^2 \theta)^{1/2}, \quad (1)$$

where d is the particle diameter, θ is the incidence angle between the light and the direction normal to the film surface, and n_{eff} is the effective refractive index. Depending on the particle diameter, light reflection can be tuned easily according to Eq. (1). Therefore, colloidal crystals are one class of the most promising candidates for light manipulation by a simple method. One primitive example of the manipulation of light using colloidal crystals is the change of structure colors. MMSS opals were fabricated from particles with different sizes ranging from 260 nm to 340 nm using fluidic cells. A wide range of structure colors from blue to pink were clearly observed, as shown in Fig. 5(c).

3. 1. 2. Control of Light Reflection Using Water Vapor Adsorption

Here, we introduce a novel strategy for the control of light reflection by taking advantage of the unique porous structure of MMSS. The highly ordered mesoporous structure of MMSS provides an effective refractive index (n_{eff}) that is changed depending on the guest molecules adsorbed in the mesopores, as shown by the XRD pattern in Fig. 1(b). For closed-packed structures (26% air) of MMSS opal, n_{eff} can be calculated from Eqs. (2) and (3):⁽³¹⁾

$$n_{\text{eff}}^2 = 0.26n_m^2 + 0.74n_{\text{MMSS}}^2, \quad (2)$$

$$n_{\text{MMSS}}^2 = \sum_i n_i^2 V_i, \quad (3)$$

where n_m and n_{MMSS} are the refractive indices of the medium (air) and MMSS. The n_{MMSS} index is defined using the volume fraction (V_i) and the refractive index (n_i) of i components, which are silica (the wall of MMSS) and the guest molecules in the mesopores (water vapor and air). These equations indicate that n_{MMSS} can be easily controlled by changing the amount of adsorbate in the mesopores, which enables light reflection to be manipulated.

Water vapor adsorption/desorption isotherms were

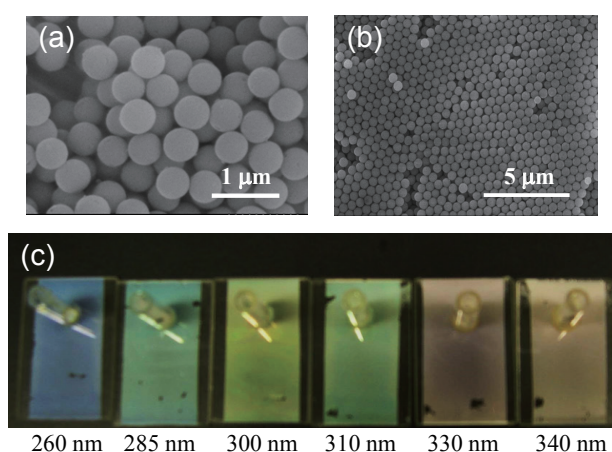


Fig. 5 SEM images of (a) MMSS and (b) a colloidal crystal film from MMSS (473 nm). (c) Photos of colloidal crystal films composed of different particle sizes of MMSS.

measured to confirm the amount of water vapor adsorbed in the mesopores of MMSS. A type V adsorption isotherm, which is typical for mesoporous materials, was confirmed, as shown in Fig. 6(a). The amount of adsorbed water vapor increases gradually until a relative pressure of ca. 0.4, and then increases sharply to reach maximum adsorption (capillary condensation). Mesopores are preferentially wet with adsorbed guest molecules due to capillary condensation, so that the water vapor can be assumed to be condensed within the mesopores, but not in the internal spaces between MMSS. Angle-resolved reflection spectra of MMSS opals were then measured at different vapor pressures using the experimental setup shown in Fig. 2. Figure 6(b) shows changes in λ_{peak} as a function of the incidence angle θ collected at $P/P_0 = 0.2$ and 0.8, where water vapor is desorbed at the former pressure

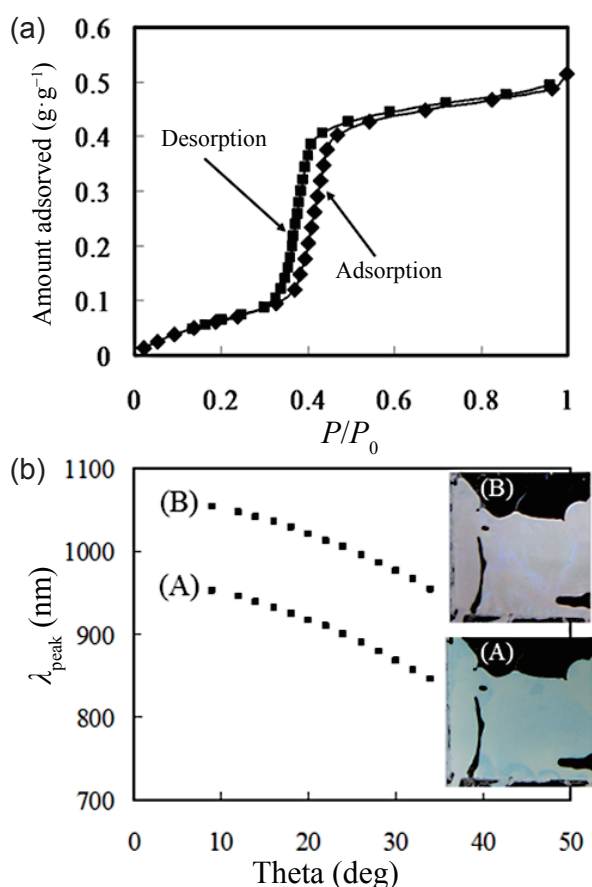


Fig. 6 (a) Adsorption/desorption isotherms of water vapor for MMSS. (b) Shifts of λ_{peak} of the reflection spectra as a function of angle θ at (A) $P/P_0 = 0.2$ and (B) $P/P_0 = 0.8$. Insets show the corresponding photos of the MMSS opal.

and adsorbed at the latter. According to Eq. (1), λ_{peak} shifts to shorter wavelength as θ increases; however, the position of λ_{peak} is clearly different depending on the relative vapor pressure. Values of λ_{peak} measured at $P/P_0 = 0.2$ were ca. 100 nm lower than those measured at $P/P_0 = 0.8$. The shift of λ_{peak} leads to an apparent difference in the structure colors between these two relative pressures, in accordance with the secondary diffraction observed in the visible wavelength range. The MMSS opal is a pale blue color at $P/P_0 = 0.2$ and changes to a pale pink color as the mesopores of MMSS are filled with water vapor at $P/P_0 = 0.8$, as shown in the insets of Fig. 6(b). It should be noted that such a color change (i.e. λ_{peak}) is reversible for over five cycles by a change in the relative vapor pressure.

The effective refractive index n_{eff} can be obtained from Eq. (1) based on angle-resolved reflection spectra measurements (denoted as n_{eff} (B)), and from Eqs. (2) and (3) using the adsorption properties (denoted as n_{eff} (A)). A comparison of n_{eff} (A) and n_{eff} (B) is tabulated in Table 1. Known refractive index values, $n_{\text{air}} = 1.00$, $n_{\text{water}} = 1.33$, and $n_{\text{silica}} = 1.46^{(32)}$ are employed, and the density of MMSS is assumed to be $1.8 \text{ cm}^3 \text{ g}^{-1}$. Using these values, n_{eff} (A) was calculated as 1.19, 1.23, and 1.29 for $P/P_0 = 0.2, 0.4,$ and 0.8 , respectively. These values are consistent with n_{eff} (B) values, which were determined to be 1.18, 1.24, and 1.29 for the different relative pressure conditions. This agreement confirms that light reflection was effectively controlled by guest molecules adsorbed in the mesopores. To the best of our knowledge, this is the first demonstration of the control of reflected light using the intrinsic adsorption properties of mesoporous synthetic opals. This feature is adaptable for optical devices to manipulate light reflection as well as sensors or indicators.

Table 1 Comparison of the refractive index n_{eff} (A) and n_{eff} (B). The n_{eff} (A) was calculated based on the adsorption property and the n_{eff} (B) was determined from angle-resolved reflection spectroscopy measurements at different P/P_0 .

| P/P_0 | n_{eff} (A) | n_{eff} (B) |
|---------|----------------------|----------------------|
| 0.2 | 1.19 | 1.18 |
| 0.4 | 1.23 | 1.24 |
| 0.8 | 1.29 | 1.29 |

3. 1. 3. Manipulation of Spontaneous Emission with Rh B-MMSS Opals

Here, we will further demonstrate the availability of MMSS opals as a promising platform to manipulate the flow of light. The utilization of MMSS opals impregnated with fluorescent guest molecules (Rh B) as an optical resonator requires consideration of whether the emission spectrum of Rh B overlaps sufficiently with the PBG of the Rh B-MMSS opals, because this is crucial for effective confinement of light emission within the PBG. To this aim, angle-resolved reflection spectra of the Rh B-MMSS opals were measured using the same apparatus employed in Sec. 2.1.4. **Figures 7(a)** and **(b)** show reflection spectra for the Rh B-MMSS opals with diameters of 320 nm (Rh B-MMSS opal_320 nm) and 564 nm (Rh B-MMSS opal_564 nm), respectively, measured at several incidence angles, together with the emission spectrum of Rh B. For Rh B-MMSS opal_320 nm, the PBG shifted to a shorter wavelength range and intersected with the emission range of Rh B. The maximum overlap was achieved at a measurement angle of 24° (Fig. 7(a)). The reflection spectra of Rh B-MMSS opal_564 nm were in the wavelength range of 900-1100 nm due to the particle size, which did not overlap with the Rh B emission at any detection angles (Fig. 7(b)). Figure 7(c) shows angle-resolved emission spectra measured for Rh B-MMSS opal_320 nm using the experimental apparatus depicted at Fig. 3 with an excitation energy of 0.04 mJ/pulse. The emission intensity for Rh B had a minimum value at an angle of 29° , where a large portion of the reflection spectra overlaps with the emission spectra of Rh B (Fig. 7(a)). It should be noted that the angle (29°) is slightly different from that at which the reflection spectrum overlaps the most with the emission spectrum of Rh B (24°). The inconsistency of these two angles may come from the difference in the measurement apparatus used for the two emission studies. Although such a disagreement may exist, the result clearly indicates that the spontaneous emission from Rh B is significantly affected by the overlap area between the reflection spectrum of the MMSS opal and the emission spectrum of the guest molecules in the mesopores. Finally, we will demonstrate the amplified spontaneous emission using the Rh B-MMSS opal. Figure 7(d) shows the dependence of the emission peak intensity on the laser power measured for the

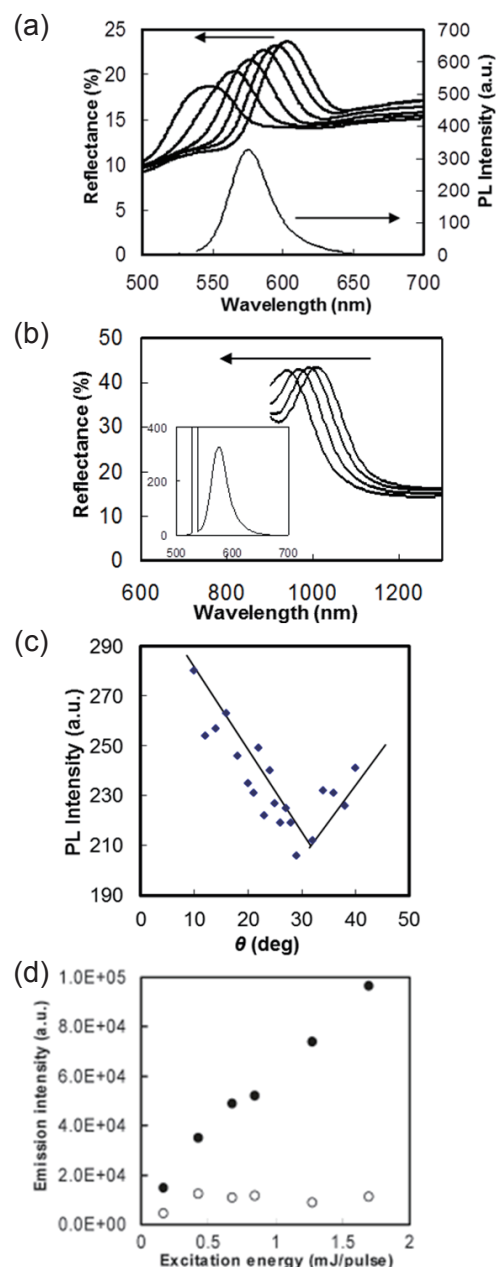


Fig. 7 Reflection spectra for (a) Rh B-MMSS opal_320 nm at angles of incidence of 12° , 16° , 20° , 24° , 28° , and 32° , and (b) Rh B-MMSS opal_564 nm at angles of incidence of 15° , 20° , 25° , and 35° . At each measurement, the rightmost spectrum is that collected at the minimum incident angle, and the spectrum shifts to the shorter wavelength region with an increase of the incident angle, as indicated by the arrow. The spectrum in the wavelength range 550-650 nm is the emission of Rh B. (c) Emission peak intensity of Rh B-MMSS opal_320 nm as a function of incident angle θ . (d) Emission peak intensity of Rh B-MMSS opal_320 nm (filled circles) and Rh B-MMSS opal_564 (open circles) as a function of excitation pulse energy.

two Rh B-MMSS opals. The emission intensity of Rh B-MMSS opal_320 nm increased with increasing laser excitation strength. When Rh B-MMSS opal_320 nm was excited at 1.7 mJ/pulse, the emission narrowed and a full width at half-maximum (FWHM) of 5 nm was achieved. Such a phenomenon was not observed for Rh B-MMSS opal_564 nm, which indicates that the spontaneously emitted light is effectively manipulated by the photonic stop band of the Rh B-MMSS opal. Both inhibited and enhanced emitted light were detected in the present Rh B-MMSS opal systems, which is expected to open novel avenues for the realization of efficient modulation of light waves by simple and cost-effective self-assembly.

3. 2. Silica Nanopillars

3. 2. 1 Transient Morphological Changes

In this section, applications of the self-assembled block copolymers for nanoscale devices are introduced. Block copolymers spontaneously self-assemble into a microphase separated structure; however, an external driving force is required to achieve the desired morphology that is appropriate for various device applications. **Figure 8** shows the transient morphological change of a microphase-separated SiO_x film with annealing time under chloroform vapor. At 5 min annealing, small isolated domains are randomly scattered, and remain almost unchanged after annealing for 60 min. Perpendicular cylindrical domains are

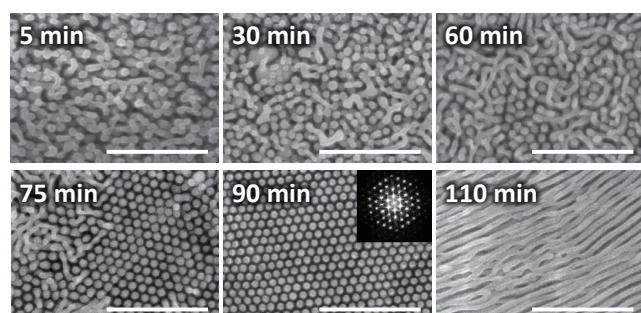


Fig. 8 Transient morphological change of SiO_2 nanopillar arrays at different annealing time in chloroform vapor. The inset is the corresponding 2D-FFT pattern. Scale bars indicate 500 nm.

mixed in the random phase when the film was annealed for 75 min. Further annealing up to 90 min yielded highly aligned perpendicular cylinders over the entire substrate. A well-developed hexagonal alignment was verified by the corresponding two-dimensional fast Fourier transformation (2D-FFT) pattern (inset of Fig. 8), which revealed bright spots with peaks up to the fifth order. The perpendicular alignment is sensitive to the annealing time as it changes to completely parallel with longer annealing time. **Figure 9** shows magnified top and cross sectional SEM images of the obtained films annealed for 90 min. A long-range regularity is confirmed in Fig. 9(a) and an array of perpendicular straight nanopillars with diameters of 30 nm and heights of 200 nm is revealed in Fig. 9(b). Thus, self-assembly of a block copolymer enables the fabrication of highly ordered nanostructures with long-range order in a simple and applicable way.

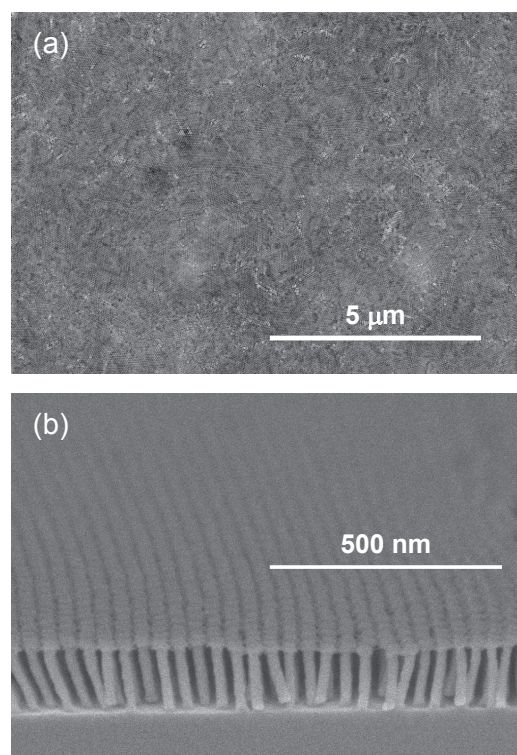


Fig. 9 Low-magnification FE-SEM images of films processed according to the scheme depicted in Fig. 4. (a) A top view of a film annealed in chloroform vapor for 90 min (before ETCH 1). (b) A cross-sectional image of SiO_2 nanopillar arrays after ETCH 2 (sample (b) in Fig. 4).

3. 2. 2 Reproducible SERS Substrates

SERS is a promising application in many fields such as chemistry, biology, and environmental science because target molecules can be detected with high sensitivity.^(33,34) SERS can be attributed to the formation of localized plasmons between closely distributed metallic nanoparticles, which gives rise to large enhancement of the electromagnetic field. For SERS applications, the stable detection of target molecules and strong enhancement of the detection intensity are important. Here, we will demonstrate that SiO₂ nanopillar arrays with high uniformity and a small domain size (i.e., the adjacent SiO₂ pillars are ca. 20 nm apart) can be employed as reproducible SERS substrates. An Au layer was evaporated onto the perpendicular SiO₂ array (sample (b) in Fig. 4), followed by introduction of R6G as a target molecule to give a SERS substrate. Raman spectra measured with the SERS substrate and that for a flat Au film are compared in Fig. 10. When the fabricated SERS substrate was irradiated, peaks were clearly observed at 1366, 1515, 1576, and 1653 cm⁻¹, which were assigned to the aromatic ring vibrations of R6G. The peak at 620 cm⁻¹ was assigned to the in-plane C-C-C ring, while the peaks at 780 cm⁻¹ and 1130 cm⁻¹ were assigned to the out-of-plane C-H and in-plane C-H bending modes,

respectively.⁽³⁵⁾ The magnitude of the Raman intensity for the SERS substrate was 250-fold greater than that for the flat Au film when the peak centered at 1653 cm⁻¹ was used for quantitative evaluation. SERS measurements were repeated at five different spots (runs 1-5 in Fig. 10), which revealed almost identical SERS spectra for the repeated runs. Highly reproducible sensitivity of the SERS substrate was thus demonstrated, which is attributable to the uniform structure of the SiO₂ nanopillars throughout the substrate. We have recently reported that SiO₂ nanopillar arrays immersed in air exhibit a uniaxial epsilon-near-zero response mediated by phonon polaritons.⁽²⁶⁾ The high-aspect ratio of the SiO₂ nanopillar achieves a uniaxial anisotropy in the direction perpendicular to the substrate, which has the potential to provide strong light-matter interaction in the mid-infrared wavelength range. Further study is underway to utilize the SiO₂ nanopillar arrays as available platforms for applications such as thermal emission control and photonic sensing to achieve nanophotonic devices for the benefit of society.

4. Conclusions

Self-assembly is utilized to fabricate nano architectures, and unique properties derived from their structures are demonstrated. Monodisperse

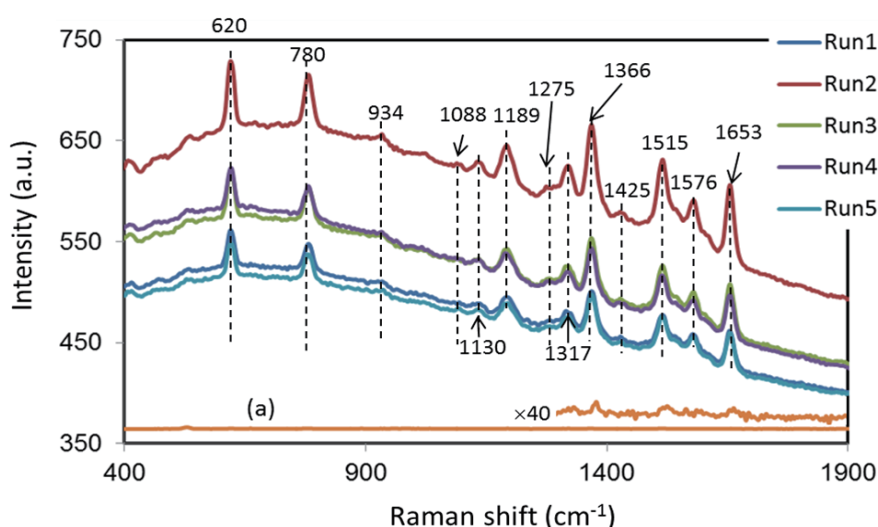


Fig. 10 Comparison of the Raman spectra of R6G molecules adsorbed on the fabricated Au/SiO₂ pillar arrays and the control Au flat substrate (labelled (a)). The measurements were repeated for five times for the Au/SiO₂ pillar arrays, confirming high reproducibility.

mesoporous silica spheres are obtained via templating the self-assembled surfactants, which can then spontaneously form colloidal photonic crystals analogous to natural gem opals. Reversible control of light reflection is investigated by changing the amount of water vapor adsorbed within the mesopores. In addition, a commonly used fluorophore, Rhodamine, was embedded in the mesopores of MMSS and the spontaneous emission from Rhodamine was manipulated. Fabrication of SiO₂ nanopillar arrays based on microphase-separated nanostructures was further demonstrated by the self-assembly of a PS-*b*-PDMS block copolymer. Highly ordered hexagonal regularity was confirmed over an entire substrate (ca. 4 cm²), which facilitated the application as a SERS substrate when Au was sputtered on the top of the SiO₂ nanopillars. Characteristic Raman signals from the target molecules adsorbed on the surface were well reproduced and the signal intensity was enhanced by 250-fold compared to that for a flat Au substrate. Fabrication of nanostructures using self-assembly strategies is simple, cost-effective, and time-efficient, thus enabling the widespread implementation of nanofabrication technology to contribute significant advances in nanotechnology.

Acknowledgments

The authors received technical assistance for Raman spectroscopy from Dr. Yuichi Kato. Discussions with Drs. Masahiko Ishii and Hiroaki Wakayama have been fruitful. This work was supported in part by the Toyota Technological Institute Nano Technology Hub of the "Nanotechnology Platform Project" sponsored by the Ministry of Education, Culture, Sports, Science and Technology (MEXT), Japan.

Finally, this paper is dedicated to the memory of our respected colleague, Dr. Kota Ito, who passed away in 2018.

References

- (1) Tans, S. J., Verschueren, A. R. M. and Dekker, C., "Room-temperature Transistor Based on a Single Carbon Nanotube", *Nature*, Vol. 393, No. 6680 (1998), pp. 49-52.
- (2) Whang, D., Jin, S., Wu, Y. and Lieber, C. M., "Large-scale Hierarchical Organization of Nanowire Arrays for Integrated Nanosystems", *Nano Lett.*, Vol. 3, No. 9 (2003), pp. 1255-1259.
- (3) Mornet, S., Elissalde, C., Bidault, O., Weill, F., Sellier, E., Nguyen, O. and Maglione, M., "Ferroelectric-based Nanocomposites: Toward Multifunctional Materials", *Chem. Mater.*, Vol. 19, No. 5 (2007), pp. 987-992.
- (4) Medintz, I. L. and Mattoussi, H., "Quantum Dot-based Resonance Energy Transfer and Its Growing Application in Biology", *Phys. Chem. Chem. Phys.*, Vol. 11, No. 1 (2009), pp. 17-45.
- (5) Lee, M., Jeon, Y., Moon, T. and Kim, S., "Top-down Fabrication of Fully CMOS-compatible Silicon Nanowire Arrays and Their Integration into CMOS Inverters on Plastic", *ACS Nano*, Vol. 5, No. 4 (2011), pp. 2629-2636.
- (6) Kiani, A., Venkatakrishnan, K., Tan, B. and Venkataramanan, V., "Maskless Lithography Using Silicon Oxide Etch-stop Layer Induced by Megahertz Repetition Femtosecond Laser Pulses", *Opt. Express*, Vol. 19, No. 11 (2011), pp. 10834-10842.
- (7) Rothmund, P. W. K., "Folding DNA to Create Nanoscale Shapes and Patterns", *Nature*, Vol. 440, No. 7082 (2006), pp. 297-302.
- (8) Shevchenko, E. V., Talapin, D. V., Kotov, N. A., O'Brien, S. and Murray, C. B., "Structural Diversity in Binary Nanoparticle Superlattices", *Nature*, Vol. 439, No. 7072 (2006), pp. 55-59.
- (9) Zhao, Y., Xie, Z., Gu, H., Zhu, C. and Gu, Z., "Bio-inspired Variable Structural Color Materials", *Chem. Soc. Rev.*, Vol. 41, No. 8 (2012), pp. 3297-3317.
- (10) Xia, F. and Jiang, L., "Bio-inspired, Smart, Multiscale Interfacial Materials", *Adv. Mater.*, Vol. 20, No. 15 (2008), pp. 2842-2858.
- (11) Gu, Z.-Z., Fujishima, A. and Sato, O., "Fabrication of High-quality Opal Films with Controllable Thickness", *Chem. Mater.*, Vol. 14, No. 2 (2002), pp. 760-765.
- (12) Yablonovitch, E., "Inhibited Spontaneous Emission in Solid-state Physics and Electronics", *Phys. Rev. Lett.*, Vol. 58, No. 20 (1987), pp. 2059-2062.
- (13) Joannopoulos, J. D., Villeneuve, P. R. and Fan, S., "Photonic Crystals: Putting a New Twist on Light", *Nature*, Vol. 386, No. 6621 (1997), pp. 143-149.
- (14) Painter, O., Lee, R. K., Scherer, A., Yariv, A., O'Brien, J. D., Dapkus, P. D. and Kim, I., "Two-dimensional Photonic Band-gap Defect Mode Laser", *Science*, Vol. 284, No. 5421 (1999), pp. 1819-1821.
- (15) Kopp, V. I., Fan, B., Vithana, H. K. M. and Genack, A. Z., "Low-threshold Lasing at the Edge of a Photonic Stop Band in Cholesteric Liquid Crystals", *Opt. Lett.*, Vol. 23, No. 21 (1998), pp. 1707-1709.
- (16) Chen, C.-Y., Li, H.-X. and Davis, M. E., "Studies on Mesoporous Materials: 1. Synthesis and Characterization of MCM-41", *Micropor. Mater.*, Vol. 2, No. 1 (1993), pp. 17-26.
- (17) Davis, M. E., "Ordered Porous Materials for Emerging Applications", *Nature*, Vol. 417, No. 6891 (2002), pp. 813-821.

- (18) Corma, A., "From Microporous to Mesoporous Molecular Sieve Materials and Their Use in Catalysis", *Chem. Rev.*, Vol. 97, No. 6 (1997), pp. 2373-2420.
- (19) Yamada, Y., Nakamura, T., Ishii, M. and Yano, K., "Reversible Control of Light Reflection of a Colloidal Crystal Film Fabricated from Monodisperse Mesoporous Silica Spheres", *Langmuir*, Vol. 22, No. 6 (2006), pp. 2444-2446.
- (20) Yamada, Y., Nakamura, T. and Yano, K., "Optical Response of Mesoporous Synthetic Opals to the Adsorption of Chemical Species", *Langmuir*, Vol. 24, No. 6 (2008), pp. 2779-2784.
- (21) Yamada, Y., Yamada, H., Nakamura, T. and Yano, K., "Manipulation of the Spontaneous Emission in Mesoporous Synthetic Opals Impregnated with Fluorescent Guests", *Langmuir*, Vol. 25, No. 23 (2009), pp. 13599-13605.
- (22) Lodge, T. P., "Block Copolymers: Past Successes and Future Challenges", *Macromol. Chem. Phys.*, Vol. 204, No. 2 (2003), pp. 265-273.
- (23) Bang, J., Jeong, U., Ryu, D. Y., Russell, T. P. and Hawker, C. J., "Block Copolymer Nanolithography: Translation of Molecular Level Control to Nanoscale Patterns", *Adv. Mater.*, Vol. 21, No. 47 (2009), pp. 4769-4792.
- (24) Yamada, Y., Ito, K., Miura, A., Iizuka, H. and Wakayama, H., "Simple and Scalable Preparation of Master Mold for Nanoimprint Lithography", *Nanotechnology*, Vol. 28, No. 20 (2017), 205303.
- (25) Yamada, Y., Ito, K., Miura, A., Harada, M., Matsunaga, T., Kato, Y., Matsui, T., Iizuka, H. and Wakayama, H., "Perpendicular SiO₂ Cylinders Fabricated from a Self-assembled Block Copolymer as an Adaptable Platform", *Eur. Polym. J.*, Vol. 107 (2018), pp. 96-104.
- (26) Ito, K., Yamada, Y., Miura, A. and Iizuka, H., "High-aspect-ratio Mushroom-like Silica Nanopillars Immersed in Air: Epsilon-near-zero Metamaterials Mediated by a Phonon-polaritonic Anisotropy", *RSC Adv.*, Vol. 9, No. 29 (2019), pp. 16431-16438.
- (27) Stöber, W., Fink, A. and Bohn, E., "Controlled Growth of Monodisperse Silica Spheres in the Micron Size Range", *J. Colloid Interface Sci.*, Vol. 26, No. 1 (1968), pp. 62-69.
- (28) Yano, K. and Fukushima, Y., "Synthesis of Mono-dispersed Mesoporous Silica Spheres with Highly Ordered Hexagonal Regularity Using Conventional Alkyltrimethylammonium Halide as a Surfactant", *J. Mater. Chem.*, Vol. 14, No. 10 (2004), pp. 1579-1584.
- (29) Ishii, M., Nakamura, H., Nakano, H., Tsukigase, A. and Harada, M., "Large-domain Colloidal Crystal Films Fabricated Using a Fluidic Cell", *Langmuir*, Vol. 21, No. 12 (2005), pp. 5367-5371.
- (30) Carlson, R. J. and Asher, S. A., "Characterization of Optical Diffraction and Crystal Structure in Monodisperse Polystyrene Colloids", *Appl. Spectrosc.*, Vol. 38, No. 3 (1984), pp. 297-304.
- (31) Park, S. H. and Xia, Y., "Assembly of Mesoscale Particles over Large Areas and Its Application in Fabricating Tunable Optical Filters", *Langmuir*, Vol. 15, No. 1 (1999), pp. 266-273.
- (32) McComb, D. W., Treble, B. M., Smith, C. J., De La Rue, R. M. and Johnson, N. P., "Synthesis and Characterization of Photonic Crystals", *J. Mater. Chem.*, Vol. 11, No. 1 (2001), pp. 142-148.
- (33) Prinz, J., Heck, C., Ellerik, L., Merk, V. and Bald, I., "DNA Origami Based Au-Ag-core-shell Nanoparticle Dimers with Single-molecule SERS Sensitivity", *Nanoscale*, Vol. 8, No. 10 (2016), pp. 5612-5620.
- (34) Chen, H.-Y., Lin, M.-H., Wang, C.-Y., Chang, Y.-M. and Gwo, S., "Large-scale Hot Spot Engineering for Quantitative SERS at the Single-molecule Scale", *J. Am. Chem. Soc.*, Vol. 137, No. 42 (2015), pp. 13698-13705.
- (35) Quyen, T. T. B., Chang, C.-C., Su, W.-N., Uen, Y.-H., Pan, C.-J., Liu, J.-Y., Rick, J., Lin, K.-Y. and Hwang, B.-J., "Self-focusing Au@SiO₂ Nanorods with Rhodamine 6G as Highly Sensitive SERS Substrate for Carcinoembryonic Antigen Detection", *J. Mater. Chem. B*, Vol. 2, No. 6 (2014), pp. 629-636.

Figs. 3 and 7

Reprinted from *Langmuir*, Vol. 25, No. 23 (2009), pp. 13599-13605, Yamada, Y., Yamada, H., Nakamura, T. and Yano, K., Manipulation of the Spontaneous Emission in Mesoporous Synthetic Opals Impregnated with Fluorescent Guests, © 2009 ACS, with permission from American Chemical Society.

Figs. 4 and 10

Reprinted from *Eur. Polym. J.*, Vol. 107 (2018), pp. 96-104, Yamada, Y., Ito, K., Miura, A., Harada, M., Matsunaga, T., Kato, Y., Matsui, T., Iizuka, H. and Wakayama, H., Perpendicular SiO₂ Cylinders Fabricated from a Self-assembled Block Copolymer as an Adaptable Platform, © 2018 Elsevier, with permission from Elsevier.

Figs. 5(a), 6(a) and Table 1

Reprinted from *Langmuir*, Vol. 24, No. 6 (2008), pp. 2779-2784, Yamada, Y., Nakamura, T., Ishii, M. and Yano, K., Reversible Control of Light Reflection of a Colloidal Crystal Film Fabricated from Monodisperse Mesoporous Silica Spheres, © 2006 ACS, with permission from American Chemical Society.

Yuri Yamada

Research Fields:

- Nanoscience and Nanotechnology
- Materials Chemistry
- Mass Spectrometry

Academic Degree: Dr.Eng.

Academic Societies:

- The Society of Polymer Science, Japan
- The Mass Spectrometry Society of Japan



Kota Ito†

Research Fields:

- Nanophotonics
- Nanoscale Heat Transfer

Academic Degree: Ph.D.

Academic Societies:

- The Japan Society of Applied Physics
- The Institute of Electrical Engineers of Japan
- The Heat Transfer Society of Japan



Tadashi Nakamura

Research Field:

- Functional Materials for Electronics and Sensor Applications

Academic Degree: Dr.Eng.

Academic Societies:

- The Chemical Society of Japan
- The Ceramic Society of Japan
- The Electrochemical Society of Japan

Award:

- Award of the Outstanding Papers Published in the JCSJ, The Ceramic Society of Japan, 2005



Atsushi Miura

Research Field:

- Microfabrication

Academic Society:

- Japan Society of Applied Physics



Kazuhiya Yano

Research Fields:

- Nanoporous Materials
- Nanocomposites
- Phonon Study

Academic Degree: Dr.Eng.

Academic Society:

- The Chemical Society of Japan



†Deceased September 2018